Published in final edited form as:
Nat Biotechnol. 2013 August ; 31(8): . doi:10.1038/nbt.2643.

Photoreceptor precursors derived from three-dimensional embryonic stem cell cultures integrate and mature within adult degenerate retina

Anai Gonzalez-Cordero[#1], **Emma L. West**[#1,*], **Rachael A. Pearson**[1], **Yanai Duran**[1], **Livia S. Carvalho**[1], **Colin J. Chu**[1], **Arifa Naeem**[1], **Samuel J. I. Blackford**[1], **Anastasios Georgiadis**[1], **Jorn Lakowski**[2], **Mike Hubank**[3], **Alexander J. Smith**[1], **James W. B. Bainbridge**[1], **Jane C. Sowden**[2], and **Robin R. Ali**[1,4,*]

[1]Department of Genetics, UCL Institute of Ophthalmology, 11-43 Bath Street, London, EC1V 9EL UK

[2]Developmental Biology Unit, University College London, 30 Guilford Street, London, WC1N 1EH UK

[3]UCL Genomics, University College London, 30 Guilford Street, London, WC1N 1EH UK

[4]Molecular Immunology Unit, Institute of Child Health, University College London, 30 Guilford Street, London, WC1N 1EH UK

[#] These authors contributed equally to this work.

Abstract

Irreversible blindness caused by loss of photoreceptors may be amenable to cell therapy. We previously demonstrated retinal repair[1] and restoration of vision through transplantation of photoreceptor precursors obtained from post-natal retinas into visually impaired adult mice[2,3]. Considerable progress has been made in differentiating embryonic stem cells (ESCs) *in vitro* toward photoreceptor lineages[4-6]. However, the capability of ESC-derived photoreceptors to integrate after transplantation has not been demonstrated unequivocally. Here, to isolate photoreceptor precursors fit for transplantation, we adapted a recently reported three-dimensional (3D) differentiation protocol that generates neuroretina from mouse ESCs[6]. We show that Rhop.GFP-selected rod precursors derived by this protocol integrate within degenerate retinae of adult mice and mature into outer segment–bearing photoreceptors. Notably, ESC-derived precursors at a developmental stage similar to postnatal days 4-8 integrate more efficiently than cells at other stages. This study shows conclusively that ESCs can provide a source of photoreceptors for retinal cell transplantation.

Many studies by our group and others have demonstrated integration into wild-type and degenerate mouse retinae of photoreceptor precursors isolated from early post-natal retinas[1-3,7-12]. Morever, we have shown that transplantation of a purified population of post-

[*]Correspondence to: Robin R. Ali (r.ali@ucl.ac.uk) or Emma L. West (e.west@ucl.ac.uk), Department of Genetics, University College London Institute of Ophthalmology, 11-43 Bath Street, London, EC1V 9EL, UK, Tel: +44 (0) 20 7608 6902, Fax: +44 (0) 20 7608 6903, http://www.ucl.ac.uk/ioo/research/ali.htm.

AUTHOR CONTRIBUTIONS A.G.C. and E.L.W. contributed equally to the concept, design, execution and analysis of all experiments and manuscript writing. R.A.P. performed subretinal transplantation and calcium imaging and contributed to the concept and design of the experiments, funding and manuscript writing. Y.D. performed subretinal transplantations and histological processing. L.S.C, A.G. and J.L. contributed to experimental execution. C.J.C performed IMARIS reconstruction. A.N and S.B. provided technical assistance. M.H. performed microarray data analysis. J.W.B.B., A.J.S., J.C.S. and R.R.A. contributed to the concept and design of the experiments, funding and to manuscript writing.

Europe PMC Funders Author Manuscripts

natal photoreceptor precursors can restore rod-mediated vision in mice[2]. Both the number of cells transplanted and the stage of their development at the time of transplantation are important parameters in achieving efficient integration[1,2]. The requisite next step toward clinical translation is to prove that pluripotent stem cell lines, which represent a renewable source of cells for transplantation, can provide equivalent transplantation-competent photoreceptor precursors. Although progress has been made in developing protocols for *in vitro* differentiation of ESCs and induced pluripotent stem cells (iPSCs) toward photoreceptor lineages[4-6,13-16], no study has unequivocally proved that ESCs can give rise to mature outer segment–bearing photoreceptors. Using an optimized adherent (2D) culture system that generates retinal cells[5,17], we were unable to demonstrate the integration of GFP-labeled mouse ESC–derived photoreceptors after transplantation[18]. These findings led us to conclude that although current 2D ESC culture systems produce cells expressing a selection of photoreceptor markers, they do not faithfully re-enact developmental processes and are therefore unlikely to provide a robust source of photoreceptor precursors equivalent to those from the developing retina.

In 2011, ground-breaking work described a 3D embryoid body–based differentiation protocol that mimicked the normal development of the embryonic retinal tissue and raised the possibility of generating authentically specified and correctly staged photoreceptors for transplantation[6,19]. Here we have optimized and scaled-up the generation of mouse ESC-derived photoreceptors in 3D synthetic retinal tissue, enabling us to transplant purified populations of photoreceptors from defined stages of development and to investigate the potential of the cells to integrate within the adult recipient retina and to mature into new photoreceptors.

A schematic of *in vitro* retinal differentiation is shown in Figure 1a. Continuous neuroepithelium-like structures were detected as early as day 5 of differentiation (Fig. 1b). At day 7, the presumptive eye fields evaginated from the embryoid bodies, forming hemispherical optic vesicle–like structures (Fig. 1c). At around day 9, the optic vesicles invaginated to form optic cup–like structures (Fig. 1d-e), and pigmented RPE cells were first detected at day 11–12 (Fig. 1f). Transparent neuroepithelia structures were still present within the embryoid bodies at later stages of culture (Fig. 1g). To investigate retinal differentiation, we quantified the number of embryoid bodies containing eye-field stage, optic vesicle and optic cup–like structures at days 5, 7 and 9 of differentiation (Fig. 1h-j, respectively). Neuroepithelium and optic vesicle–like structures decreased from day 5 to 9 in culture (Fig. 1h,i, respectively), but the proportion of optic cup–like structures, characterized by a hinge region, increased significantly over the same period (Fig. 1j). Although an incomplete invagination was observed in some instances, this did not interfere with further neural retinal specification and photoreceptor differentiation, similar to other studies using human ES and iPS cells[15,16]. Unlike the protocol used by Eiraku *et al.*[6], we kept EBs as intact structures, referred to here as whole EBs (wEBs), for the entire period of differentiation as manual excision of optic cup–like structures from the EBs did not allow the scaling up required to produce large numbers of transplantable photoreceptors. In addition, in contrast to the earlier protocol[6], wEB cultures were grown under atmospheric oxygen levels ($20\%O_2$;$5\%CO_2$). At day 9-12 of differentiation, optic cup–like structures demonstrated apical-basal polarity, with the apical side facing the interior of the wEB. Large numbers of dividing cells were observed, and mitosis occurred at the apical surface (Supplementary Fig. 1). Similar to eye development *in vivo*, the majority of cells within the ESC-derived neuroepithelia analyzed between days 7-12 expressed Rax, Pax6 and Vsx2 (Chx10), indicating that they were proliferating retinal progenitor cells (RPCs) (Supplementary Fig. 2a-d). Also similar to development *in vivo*, co-localization of Pax6 and Mitf was widespread throughout the neuroepithelium of day 7 optic vesicles (Supplementary Fig. 2e-h). $Mitf^+$ RPE progenitors became progressively restricted to defined proximal

portions of the invaginating neuroepithelium by day 12 (Supplementary Fig. 2i,j). Retinal differentiation was further confirmed by RT-PCR analysis of eye field transcription factors and RPC markers between day 0 and day 16 of differentiation (Supplementary Fig.2l). From day 14 onwards, wEBs were cultured in serum-free conditions and in the presence of retinoic acid (RA) and Taurine, factors reported to promote rod photoreceptor fate[20-22]. These conditions increased expression of rod-specific genes compared with both pulse application of RA and Taurine between days 14-16 of differentiation and culturing with FBS throughout the culture period (Supplementary Fig. 3).

We next determined whether the RPCs generated using our 3D wEB differentiation system were capable of further differentiation into mature retinal cell types, despite the presence of other non-retinal neuronal and glial cell types (Supplementary Fig. 4). At day 26 of culture, markers for ganglion, amacrine, horizontal and bipolar cells were found in a single layer at the basal side of the optic cup–like structures. Photoreceptors were observed in a well-developed ONL-like layer (Supplementary Fig. 5) and robust expression of a variety of photoreceptor-specific markers was detected (Fig. 1k). By day 24 of culture, increasing from day 20, the majority of cells in the wEB expressed Crx, a marker of post-mitotic photoreceptor precursors (Fig. 1l-o). All wEBs examined contained at least one neural retina–like region, and these, without exception, expressed markers of photoreceptor differentiation (n >500 EBs). Rod photoreceptors were abundant, and very few cones could be detected.

We sought to determine how closely ESC-derived photoreceptor development within the 3D system compared with normal photoreceptor development *in vivo* by analyzing the time-course of expression of a number of photoreceptor-specific markers in ESC-derived photoreceptors and photoreceptors from post-natal retinas. There is a peak of *Crx* expression between P3-P6 in the early post-natal retina, which is down-regulated in more mature photoreceptors[23-25]. Similarly, we showed a marked increase in the number of Crx^+ photoreceptor precursors between days 20 and 24, which decreased after day 26 of culture (Fig. 2a). The reduction in Crx was accompanied by a significant increase in Rhodopsin and Recoverin (Fig. 2a), placing day 26 of culture at a stage similar to P4-P6 stage of development (Supplementary Fig.6). *In vivo,* both rod α-Transducin (Gnat1) and Peripherin-2 protein levels increased substantially between P8 and P12, coincident with the onset of outer-segment formation (Fig. 2b,c). A similar pattern was observed *in vitro*; at day 28 there were few positively labeled cells, but by day 36 the majority of cells were rod α-Transducin and Peripherin-2 positive (Fig. 2d,e, respectively).

To further analyze the degree of similarity between the differentiation states of ESC-derived rods and donor-derived rod photoreceptors, we compared gene expression profiles by microarray analysis. We used an adeno-associated viral vector (pseudotype 2/9) carrying a GFP reporter under the control of a *Rhodopsin* promoter (AAV2/9.Rhop.GFP) (Fig. 2f) to select the rod photoreceptors. AAV2/9.Rhop.GFP^+ rods were sorted by fluorescence-activated cell sorting (FACS) at days 26 and 34 of culture and post-natal stage P12 (Supplementary Fig.7). The ESC-derived populations (day 26 and 34) expressed genes enriched in transplantation-competent P4 rod photoreceptor precursors[10] consistent with photoreceptor cell differentiation. Day 34 cultures showed higher expression of genes encoding structural components of outer segments and phototransduction, such as *Gnat1*, *Rho*, *Pde6a*, *Prph2*. Hierarchical cluster analyses demonstrated that the day 34 Rhop.GFP^+ cells were more mature as they more closely resembled (transplantation incompetent) P12 photoreceptors than the earlier-stage day 26 cells (Fig. 2g). Therefore, we sought to establish whether these late postnatal AAV2/9.Rhop.GFP^+ rods formed outer segments. Peripherin-2, a marker for outer segments *in vivo*, was located to the segment region of the ESC-derived rods (Fig. 2h,i high magnification, arrow head). However, although ultrastructural

examination of day 36 wEBs demonstrated the presence of inner-segment and cilium-like structures, no outer segments were observed (Fig. 2j, arrow head). Cross-sections of these structures showed inner segments packed full of mitochondria (Fig. 2j, continuous line and **k**, asterisks) and a typical photoreceptor cilium, which contained the 9+0 microtubular arrangement (Fig. 2j, dashed line and **l**). Together, these findings confirm the survival and differentiation of wEBs 3D-derived photoreceptors to a stage equivalent to late post-natal development.

We next examined the capability of ESC-derived photoreceptor precursors generated using our wEBs 3D differentiation protocols to integrate into adult retina and form new mature photoreceptors. A robust evaluation of the integration and maturation capability of ESC-derived cells was achieved by assessing expression of outer-segment proteins following transplantation in recipient retinae deficient in these proteins. We transplanted 200,000 AAV2/9.Rhop.GFP$^+$ FAC-sorted precursors (day 26-29) via subretinal injection into the adult *Gnat1*$^{-/-}$ mouse, a model of stationary night blindness, which lack rod function because of the absence of rod α-Transducin phototransduction protein[26]. Three weeks after transplantation, Rhop.GFP$^+$ sorted photoreceptor precursors had migrated and integrated into the recipient ONL (Fig. 3a). Integrated ESC-derived rods were correctly oriented within the ONL and were usually found in small clusters, a characteristic frequently seen in transplants using donor-derived photoreceptor precursors[2,9]. Moreover, integrated rods displayed morphological features typical of mature photoreceptors, including inner and outer segments projected towards the host RPE (Fig. 3a) and rod spherules in the OPL (Fig. 3b, arrow heads). The identity and number of the integrated ESC-derived photoreceptors was established by counting GFP$^+$ cells that also expressed rod α-Transducin (Rhop.GFP$^+$/Gnat1$^+$). Integrated rods were found predominantly around the cell mass, near the injection site (Fig. 3c), and these cells were still present 6 weeks after transplantation.

Previously, transplanted human ESC-derived cultures labeled with GFP viruses were reported to integrate within adult mouse retinae. These integrated cells resembled mouse photoreceptor cells in size and outer segments did not form following transplantation in the *Crx*$^{-/-}$ mouse model[27]. As we recently demonstrated that it is possible for contaminating viral particles to be co-injected with transplanted cells and to label endogenous photoreceptors[18], potentially leading to false-positive results, we formally excluded this possibility in our experiments. To determine the number of virus-labeled host photoreceptors following transplantation, we used a control ESC-derived CBA.YFP$^+$ FAC-sorted neuronal population transduced with an AAV2/9.Rhop.RFP virus and quantified the YFP$^-$/RFP$^+$ photoreceptors. Transplantation of CBA.YFP$^+$/Rhop.RFP$^-$ FAC-sorted cells resulted in a negligible number of virally transduced host photoreceptors (8 ± 2 photoreceptors per retina, n=16). Without FAC-sorting we noted significantly greater numbers of viral-labeled host photoreceptors following transplantation (113 ± 29 vs 8±2, photoreceptors; Mann-Whitney U, $p<0.0001$, $n \geq 8$) (Supplementary Fig. 8a-c). Moreover, we also examined the transplantation of unsorted ESC-derived mixed populations containing AAV2/9.Rhop.GFP$^+$ rods. We observed 113±25 GFP-labeled photoreceptors in the recipient ONL. However, only a small percentage of these cells (1±0.6%) were verified to be ESC-derived Rhop.GFP$^+$/Gnat1$^+$ integrated photoreceptors, suggesting that the majority of Rhop.GFP$^+$/Gnat1$^-$ cells were endogenous virus-labeled photoreceptors (Supplementary Fig. 8d,e). In contrast, the transplantation of a pure FAC-sorted Rhop.GFP$^+$ population showed 80% of ESC-derived Rhop.GFP$^+$ integrated rods were also Gnat1$^+$, similar to P4-8 Nrlp.GFP$^+$ donor-derived transplants (Supplementary Fig. 9). These experiments highlight the importance of stringent controls to identify true ESC-derived integrated photoreceptors.

Early post-natal rod precursors integrate into the host ONL with greater efficiency than embryonic, late post-natal or adult mature photoreceptors[1]. To determine whether ESC-

derived photoreceptor precursors behave in a similar manner, we transplanted FAC-sorted Rhop.GFP$^+$ cells at stages equivalent to early post-natal (day 26 and 29) and late post-natal (day 34) retina. The number of integrated Rhop.GFP$^+$/Gnat1$^+$ photoreceptors from day 26 (420±98 photoreceptors, n=16) and 29 (236±44 photoreceptors, n=19) cultures was significantly greater than those obtained from day 34 cultures ($P<0.05$, ANOVA; 30±6 photoreceptors, n=24) (Fig. 3d and Supplementary Fig. 9b), indicating that the developmental stage of the donor photoreceptor is important in determining its ability to integrate. We have recently shown, by transplanting Nrlp.GFP$^+$ rods derived from the early post-natal retina into mouse models of degeneration, that different diseased environments have a marked impact on the morphology of transplanted photoreceptors[3]. To confirm the identity of the ESC-derived integrated rods in other models lacking endogenous, photoreceptor-specific proteins and to determine whether ESC-derived precursors can integrate into different disease environments, we transplanted day 29 Rhop.GFP$^+$ cells into two additional models of inherited retinal degeneration. Compared with transplantation into *Gnat1*$^{-/-}$ mice, far fewer ESC-derived rods integrated into the ONL of 2-month-old peripherin-2 null mutant (*Prph2*$^{rd2/rd2}$) mice and 3-week-old rhodopsin knockout (*Rho*$^{-/-}$) mice (Supplementary Fig 10). Transplanted rods integrated within the *Gnat1*$^{-/-}$ recipient were able to form long outer segments (Fig. 3e). In contrast, integrated cells in the *Prph2*$^{rd2/rd2}$ and *Rho*$^{-/-}$models formed shorter segments (Fig. 3f,g respectively), in accordance with our previous findings transplanting donor-derived precursors[3]. Notably, ESC-derived photoreceptors expressed the outer-segment proteins missing in the endogenous rods in each of the respective knock-out models examined.

To establish whether integrated ESC-derived rod precursors were able to connect with the existing retinal circuitry, we examined transplanted eyes for the presence of synapses. Integrated Rhop.GFP$^+$ photoreceptors extended basal processes that terminated as round synaptic bouton-like structures that were in close proximity to the afferent terminals of PKC □$^+$ rod bipolar cells in the OPL (Fig. 3h). These synapse-like structures expressed the rod ribbon synapse markers Dystrophin and Ribeye (Fig. 3i,j). 3D reconstruction of individual integrated cells in retinal flat mounts demonstrated the correct morphology and anatomical localization of integrated Rhop.GFP$^+$/Gnat1$^+$ cells and highlighted the correct spatial alignment and morphology of the ribbon synapse in relation to the rod spherule (Fig. 3j-m and Supplementary movie 1).

Finally, we assessed whether the transplanted cells could respond to pharmacological stimuli in a manner similar to endogenous rods. In the ONL, the metabotropic glutamate receptor mGluR8 is expressed on photoreceptor pre-synaptic terminals, and its activation leads to a characteristic decrease in intracellular calcium in these cells[28,29] (Fig. 3n-p). (S)-3,4-dicarboxyphenylglycine (DCPG), an agonist with high specificity for the mGluR8 subtype, consistently evoked appropriate decreases in intracellular calcium in both endogenous *Gnat1*$^{-/-}$ rods and integrated ESC-derived Rhop.GFP$^+$ precursor cells that were virtually indistinguishable from those seen in wildtype rods (Fig. 3n,o), both in their profile and in the proportion of cells responding. In all cases, these decreases could be blocked by the mGluR8-specific antagonist (RS)-a-cyclopropyl-4-phosphonophenylglycine (CPPG) (Fig. 3n,o). Conversely, specific agonists of another glutamate receptor, the N-methyl-D-aspartate (NMDA) receptor, which is expressed by other retinal neurons but not by photoreceptors, had no effect (Fig. 3n).

In this study, we have demonstrated that it is possible to isolate a population of pure, ESC-derived photoreceptor precursors from 3D-cultured retinae that have the capacity to integrate and mature into new photoreceptors within a recipient retina following transplantation. Notably, we establish that rods obtained from stages in culture similar to postnatal days 4-8 integrate more efficiently than mature rods expressing later phototransduction markers.

Compared with photoreceptors obtained from our previously described 2D method, the 3D-differentiated cells expressed significantly greater levels of post-natal rod genes (Supplementary Fig. 11), supporting our hypothesis that developmental stage is key for photoreceptor integration[18]. Here, the ESC origin of the integrated photoreceptors was verified by detection of proteins absent in the photoreceptors of the recipient retinae in three different disease models. We also confirmed that transplantation of a heterogeneous population of ESC-derived cells leads to greatly reduced numbers of integrated photoreceptors, consistent with our earlier observations in transplanting donor-derived cells[2,18].

In our experiments we transplanted 200,000 ESC-derived photoreceptor precursors and observed 0.3% of these cells integrating into the retina. The number of integrated photoreceptors and their morphology were similar to those in our earlier studies using donor-derived photoreceptor precursors[1,9,30]. Assessment of visual function will require further optimization to achieve higher numbers of integrating cells. Based on our earlier work, reliable electroretinographic responses are achieved only with rescue of 150,000 functioning rods. Restoration of visual function was demonstrated in the *Gnat1*$^{-/-}$ model containing an average of 25,000 integrated cells (via water maze and Optomotry), yet electroretinographic responses were not detectable even with this number of new cells[2]. We find it difficult to reconcile our findings with previous reports of restoration of mouse electroretinographic responses with as few as 3,000 integrated human ESC-derived Nrl^{+} cells that do not form outer segments or with transplants of mixed cell populations derived from mouse iPSCs[27,31].

In conclusion, the 3D culture system described here provides a robust and consistent method of differentiating ES cells into photoreceptor precursors that can integrate into the degenerate adult mouse retina after transplantation. Our data now demonstrate unequivocally that ESC-derived photoreceptor precursor cells have the capability to integrate and mature to form outer segments and synaptic connections after transplantation into the degenerate adult mouse retina. We present clear evidence to support the utility of ESC-derived cells for photoreceptor replacement therapy. Similar 3D protocols have been developed to generate photoreceptors from human ESCs[32]; future transplantation studies will seek to establish that similar integration can be achieved using human cells.

METHODS

3D ESC retinal differentiation culture

A mouse EK.CCE ES cell line[33] (129/SvEv; a kind gift of Professor E. Robertson) was maintained as previously described[18]. For 3D retinal differentiation, 3×10^4 dissociated ES cells were resuspended per millilitre of differentiation medium (GMEM containing 1.5% KSR, 0.1mM NEAA, 1mM pyruvate, 0.1mM 2-mercaptoethanol), plated into 96 well low-binding (Corning) plates and incubated at 37°C, 5% CO_2. Embryoid body cell aggregates (EBs) formed within 24 hrs, on day 1 of culture, growth factor reduced Matrigel (BD Bioscience) was added to each well to give a final concentration of 2%. For whole EB retinal differentiation, EBs were transferred into retinal maturation medium (DMEM/F12 Glutamax containing N2 supplement and Pen/strep) at day 9, plated in low-binding plates at a density of 6 EBs/cm^2 and incubated at 37°C, 5% CO_2. The media was changed every 2-3 days, with the addition of 1mM Taurine (Sigma) and 500nM retinoic acid (Sigma) from day 14 of culture onwards. For quantification of early stages in culture the following criteria were used: neuroepithelia was characterized by a continuous neuroepithelium around the whole circumference of the EB; optic vesicle–like structures contained thickened regions of neuroepithelium that protruded from the EB; optic cup–like structures included complete and incomplete invaginated EBs and were characterized by the presence of a hinge region.

For further retinal differentiation EBs were transferred to fresh low-binding plates at day 27 of culture, at a density of 3 EBs/cm^2, with 50% media changes every 2-3 days. For experiments quantifying the number of host viral labelled photoreceptors, a CBA.YFP ES cell line (a variant of R1 ES cells; 7AC5/EYFP, from ATCC) was differentiated using the protocol above.

Production of recombinant AAV2/9 Rhop.GFP/RFP

A pD10/*Rhodopsin* promoter-*GFP or* pD10/*Rhodopsin* promoter-*RFP* construct containing AAV-2 inverted terminal repeats was used to generate AAV2/9 Rhop.GFP or Rhop.RFP. Recombinant AAV2/9 serotype particles were produced through a previously described tripartite transfection method into HEK293T cells[34], followed by purification using ion exchange chromatography[35]. Viral particle titres were determined using dot-blot analysis of purified virus DNA and plasmid controls of known concentrations. EBs were infected at day 22 of culture with 1×10^{10} viral particles per EB in retinal maturation medium.

FACS analysis

EBs were dissociated with 0.25% Trypsin at various timepoints and FAC-sorted for Rhop.GFP$^+$ or CBA.YFP$^+$/Rhop.RFP$^-$ cells, and collected in retinal maturation medium containing 10% FBS, for further analysis. Cell sorting was performed on a MoFlo XDP (Beckman Coulter) fitted with a 200mW 488nm blue laser (adjusted to 150mW) to excite GFP and RFP. GFP was collected in the 530/40nm channel and RFP in the 613/20nm channel.

Real-time and RT-PCR analysis

RNA was extracted with RNeasy Micro/Mini Kit (QIAGEN) and reverse-transcribed using QuantiTect Reverse Transcription Kit (QIAGEN). The cDNA was amplified with gene-specific primers (Supplementary Table 1). PCRs were conducted using at least 3 separate RNA preparations. Real-time quantitative RT-PCR was performed with a thermal cycler (7900HT; Applied Biosciences) as previously described[18]. Reagents were obtained from Roche Diagnostics and primers were designed for specific probe-binding regions using the Roche Universal Probe Library. Samples were run in triplicate and at least 3 independent differentiation cultures were analysed.

Microarray

AAV2/9. Rhodopsin.GFP virus was subretinally injected in P2-P4 wildtype mice and day 22 wEBs. Three independent experiments were used to obtain P12, day 26 and 34 rod precursors, which were dissociated as described above and isolated by FACs. Total RNA was isolated using a mirVana miRNA Isolation Kit (Ambion) and labeled for Affymetrix whole transcriptome microarray analysis using the Ambion WT expression kit (Invitrogen) and Affymetrix Mouse Gene 1.0 ST genechips. Raw data was normalized using RMA in Expression Console 1.2. Array QC (PCA, signal distribution and controls) was performed using Expression Console and Bioconductor. Microarray data are available in the ArrayExpress database (www.ebi.ac.uk/arrayexpress) under accession numbers E-MEXP-3921 and E-MEXP-3922. Hierarchical clustering and heat map representations were performed using GeneSpring 12.5.

Photoreceptor transplantation

C57Bl/6J (Harlan, UK), *Gnat1*$^{-/-}$ (J. Lem, Tufts University School of Medicine), *Prph2*$^{rd2/rd2}$ (G. Travis, UCLA), *Rho*$^{-/-}$ (P. Humphries, Trinity College Dublin) and *Nrlp.GFP*$^{+/+}$ (A. Swaroop, University of Michigan) mice were maintained in the animal facility at University College London. Experiments were conducted in accordance with the

Policies on the Use of Animals and Humans in Neuroscience Research, revised and approved by the ARVO statement for the Use of Animals in Ophthalmic and Vision Research. For the dystrophic models, *Gnat1*$^{-/-}$ mice received transplanted cells at 8-12 weeks of age, *Rho*$^{-/-}$ mice (n=10) at 3-4 weeks and *Prph2*$^{rd2/rd2}$ mice (n=8) at 8 weeks of age. This was in keeping with the optimal recipient age as determined by donor-derived precursor cell transplantation into these dystrophic models. All mice were kept on a standard 12hr light-dark cycle. EBs from various stages of culture were dissociated and FAC-sorted as described above and Rho.GFP^{+} cells were re-suspended at a concentration of 200,000 cells/ □ in sterile HBSS and DNase (0.05%) prior to injection. Animals were anaesthetised and surgery was performed under direct ophthalmoscopy, as described previously[1,2,18,35]. Mice were sacrificed 3 weeks after transplantation.

Immunohistochemistry

Whole EBs and eye cups were fixed for 1 hour in 4% paraformaldehyde (PFA) and embedded in OCT (RA Lamb). Cryosections were cut (18 □m thick) and all sections were collected for analysis. For immunohistochemistry, sections were blocked in 5% goat serum and 1% bovine serum albumin in PBS. Primary antibody (Supplementary Table 2) was incubated overnight at 4°C. Sections were incubated with secondary antibody for 2 hrs at RT, washed and counter-stained with DAPI (Sigma-Aldrich). Retinal flatmounts were stained by adapting a published protocol[36]. Following dissection, the retinae were placed into 100% methanol overnight, then blocked and stained in 1% BSA (Sigma-Aldrich), 3% Triton X-100 and 5% goat serum. Alexa fluor 488, 546 and 633 secondary antibodies (Invitrogen-Molecular Probes) were used at a 1:500 dilution.

Image acquisition

Retinal section and flatmount images were acquired by confocal microscopy (Leica DM5500Q). A series of XY optical sections, 1.0 □m apart, throughout the depth of the section were taken and built into a stack to give a projection image. LAS-AF image software was used. 3D reconstruction of high-resolution Z-stack images was performed with Imaris software (Bitplane).

Electron Microscopy

EBs were fixed in 3% glutaraldehyde/1% PFA at 4°C for 48 hrs and processed, as previously described[9,18,37]. Briefly, following osmium fixation and ethanol dehydration, the specimens were embedded in araldite and cured at 60°C. Semithin (0.7 □m) and ultrathin (0.07 □m) sections were cut using a Leica ultracut S microtome fitted with an appropriate diamond knife (Diatome histoknife Jumbo/Ultrathin). Ultrathin sections were collected on copper grids (100 mesh, Agar Scientific), contrast-stained with 1 % uranyl acetate and lead citrate and analysed using a JEOL 1010 Transmission Electron Microscope (80kV).

Calcium Imaging

Calcium imaging was performed using methods described previously[1] with minor modifications. Briefly, whole-mount neural retinas were loaded with Fura-Red AM (15mM, Molecular Probes)/Pluronic Acid F127 (0.03% w/v, Sigma) in artificial cerebrospinal fluid (ACSF), which contained in mM: 119.0 NaCl, 26.2 HEPES, 11 D-glucose, 2.5 KCl, 1.0 K_2HPO_4, 2.5 $CaCl_2$, 1.3 $MgCl_2$ for 1hr at 37°C and then de-esterified in ACSF alone for 30 mins at 37°C. Retinas were transferred to an inverted microscope (SP2, Leica) and held flat under a nylon-strung platinum wire ‘harp’, photoreceptor side down, and perfused with oxygenated ACSF (36°C) using a pressurized perfusion system (Harvard Apparatus Ltd). Drugs were applied via the perfusion system and included DCPG ((S)-3,4-dicarboxyphenylglycine, 40mM), CPPG ((RS)-alpha-cyclopropyl-4-

phosphonophenylglycine, 100mM) and NMDA (N-methyl-D-aspartate, 200mM) (all Tocris). GFP^+ cells were located using epifluorescence before taking confocal XY images of DAPI, GFP and Fura-Red AM to confirm the location of GFP^+ cells within the recipient ONL. Only cells with a highly condensed nucleus (typical of rods) located within the recipient ONL were included in the analysis. Fura-Red fluorescence was acquired at 4 sec intervals and analyzed off-line. NB, when excited at 488nm, the emission of Fura-Red undergoes a *increase* in fluorescence as $[Ca^{2+}]_i$ *decreases*. Endogenous GFP^- rods were randomly selected from the Hoechst image. Changes in fluorescence were normalized against the fluorescence at time 0s and a change of >10% above baseline was considered a response. Analysis was performed masked such that only the timing, not the identity of the drug applied was known at the time of analysis.

Cell counts

Counts of integrated cells were taken 3 weeks after transplantation using a fluorescence microscope (ObserverZ.1, Zeiss). The average number of integrated cells per eye was determined by counting all the integrated $Rhop.GFP^+$ cells or rod α-$Transducin^+$ cells in alternate serial sections through each eye. This was doubled to give an estimate of the mean number of integrated cells per eye. Cells were considered to be integrated if the whole cell body was correctly located within the outer nuclear layer, and at least one of the following was visible; spherule synapse, inner/outer processes, inner/outer-segments. Animals were omitted from quantification analysis only if there was clear evidence of an injection occurring intravitreally or if no cell mass was evident in the subretinal space. Counts were performed masked such that the identity of the transplanted cells was not known.

Statistical analysis

All means are presented ± SEM (standard error of the mean), unless otherwise stated; N, number of animals or independent experiments performed; n, number of eyes or EBs examined, where appropriate. For assessment of integration efficiency, statistical analysis is based on at least three independent transplantation sessions (cell preparation, FAC-sorting and transplantation). Statistical significance was assessed using Graphpad Prism 5 software and denoted as $P<0.05$= *, $P<0.01$= ** and $P<0.001$= ***. Appropriate statistical tests were applied including t-test, Mann-Whitney U and ANOVA with Tukey's correction for multiple comparisons.

Supplementary Material

Refer to Web version on PubMed Central for supplementary material.

Acknowledgments

This work was supported by the Medical Research Council UK (mr/j004553/1, G0901550), RP Fighting Blindness (GR566), The Miller's Trust and Moorfields Eye Charity through a generous donation by Mr Otto van der Wyck. A.G.C is a Wellcome Trust PhD student (087256/Z08/Z). R.A.P. is a Royal Society University Research Fellow. J.C.S. is supported by Great Ormond Street Hospital Children's Charity. R.R.A is partly funded by the Department of Health's National Institute for Health Research Biomedical Research Centre at Moorfields Eye Hospital and Alcon Research Institute. We thank A. Eddaoudi, A. Rose, T. Adejumo for FACS assistance, S. Azam and S. Haria for virus purification, S. Sharma for performing the Affymetrix microarray and P. Munro for EM assistance.

References

1. Maclaren RE, et al. Retinal repair by transplantation of photoreceptor precursors. Nature. 2006; 444:203–207. [PubMed: 17093405]
2. Pearson RA, et al. Restoration of vision after transplantation of photoreceptors. Nature. 2012; 485:99–103. [PubMed: 22522934]

Europe PMC Funders Author Manuscripts

3. Barber AC, et al. Repair of the degenerate retina by photoreceptor transplantation. PNAS. 2013; 110:354–359. [PubMed: 23248312]
4. Lamba DA, Karl MO, Ware CB, Reh TA. Efficient generation of retinal progenitor cells from human embryonic stem cells. PNAS. 2006:1–6.
5. Osakada F, et al. Toward the generation of rod and cone photoreceptors from mouse, monkey and human embryonic stem cells. Nat Biotechnol. 2008; 26:215–224. [PubMed: 18246062]
6. Eiraku M, et al. Self-organizing optic-cup morphogenesis in three-dimensional culture. Nature. 2011; 472:51–56. [PubMed: 21475194]
7. Bartsch U, et al. Retinal cells integrate into the outer nuclear layer and differentiate into mature photoreceptors after subretinal transplantation into adult mice. Experimental Eye Research. 2008; 86:691–700. [PubMed: 18329018]
8. Lakowski J, et al. Cone and rod photoreceptor transplantation in models of the childhood retinopathy Leber congenital amaurosis using flow-sorted Crx-positive donor cells. Human Molecular Genetics. 2010; 19:4545–4559. [PubMed: 20858907]
9. Pearson RA, et al. Targeted Disruption of Outer Limiting Membrane Junctional Proteins (Crb1 and ZO-1) Increases Integration of Transplanted Photoreceptor Precursors Into the Adult Wild-Type and Degenerating Retina. Cell Transplantation. 2010; 19:487–503. [PubMed: 20089206]
10. Lakowski J, et al. Effective Transplantation of Photoreceptor Precursor Cells Selected Via Cell Surface Antigen Expression. Stem Cells. 2011; 29:1391–1404. [PubMed: 21774040]
11. Eberle D, Schubert S, Postel K, Corbeil D, Ader M. Increased integration of transplanted CD73-positive photoreceptor precursors into adult mouse retina. Investigative Ophthalmology & Visual Science. 2011; 52:6462–6471. [PubMed: 21743009]
12. Singh MS, et al. Reversal of end-stage retinal degeneration and restoration of visual function by photoreceptor transplantation. PNAS. 2013; 110:1101–1106. [PubMed: 23288902]
13. Meyer JS, et al. Modeling early retinal development with human embryonic and induced pluripotent stem cells. PNAS. 2009; 106:16698–16703. [PubMed: 19706890]
14. Hirami Y, et al. Generation of retinal cells from mouse and human induced pluripotent stem cells. Neuroscience Letters. 2009; 458:126–131. [PubMed: 19379795]
15. Meyer JS, et al. Optic Vesicle-like Structures Derived from Human Pluripotent Stem Cells Facilitate a Customized Approach to Retinal Disease Treatment. Stem Cells. 2011; 29:1206–1218. [PubMed: 21678528]
16. Phillips MJ, et al. Blood-derived human iPS cells generate optic vesicle-like structures with the capacity to form retinal laminae and develop synapses. Investigative Ophthalmology & Visual Science. 2012; 53:2007–2019. [PubMed: 22410558]
17. Osakada F, Ikeda H, Sasai Y, Takahashi M. Stepwise differentiation of pluripotent stem cells into retinal cells. Nat Protoc. 2009; 4:811–824. [PubMed: 19444239]
18. West EL, et al. Defining the integration capacity of embryonic stem cell-derived photoreceptor precursors. Stem Cells. 2012; 30:1424–1435. [PubMed: 22570183]
19. Ali RR, Sowden JC. Regenerative medicine: DIY eye. Nature. 2011; 472:42–43. [PubMed: 21475187]
20. Hyatt GA, Schmitt EA, Fadool JM, Dowling JE. Retinoic acid alters photoreceptor development in vivo. Proceedings of the National Academy of Sciences of the United States of America. 1996; 93:13298–13303. [PubMed: 8917585]
21. Kelley MW, Williams RC, Turner JK, Creech-Kraft JM, Reh TA. Retinoic acid promotes rod photoreceptor differentiation in rat retina in vivo. Neuroreport. 1999; 10:2389–2394. [PubMed: 10439469]
22. Lombardini JB. Taurine: retinal function. Brain Res. Brain Res. Rev. 1991; 16:151–169. [PubMed: 1760655]
23. Chen S, et al. Crx, a novel Otx-like paired-homeodomain protein, binds to and transactivates photoreceptor cell-specific genes. Neuron. 1997; 19:1017–1030. [PubMed: 9390516]
24. Furukawa T, Morrow EM, Cepko CL. Crx, a novel otx-like homeobox gene, shows photoreceptor-specific expression and regulates photoreceptor differentiation. Cell. 1997; 91:531–541. [PubMed: 9390562]

25. Blackshaw S, et al. Genomic Analysis of Mouse Retinal Development. Plos Biol. 2004; 2:e247. [PubMed: 15226823]
26. Calvert PD, et al. Phototransduction in transgenic mice after targeted deletion of the rod transducin alpha -subunit. Proceedings of the National Academy of Sciences of the United States of America. 2000; 97:13913–13918. [PubMed: 11095744]
27. Lamba DA, Gust J, Reh TA. Transplantation of human embryonic stem cell-derived photoreceptors restores some visual function in Crx-deficient mice. Cell stem cell. 2009; 4:73–79. [PubMed: 19128794]
28. Koulen P, Kuhn R, Wässle H, Brandstätter JH. Modulation of the intracellular calcium concentration in photoreceptor terminals by a presynaptic metabotropic glutamate receptor. Proceedings of the National Academy of Sciences of the United States of America. 1999; 96:9909–9914. [PubMed: 10449793]
29. Koulen P, Brandstätter JH. Pre- and Postsynaptic Sites of Action of mGluR8a in the mammalian retina. Investigative Ophthalmology & Visual Science. 2002; 43:1933–1940. [PubMed: 12037002]
30. West EL, et al. Pharmacological disruption of the outer limiting membrane leads to increased retinal integration of transplanted photoreceptor precursors. Experimental Eye Research. 2008; 86:601–611. [PubMed: 18294631]
31. Tucker BA, et al. Transplantation of adult mouse iPS cell-derived photoreceptor precursors restores retinal structure and function in degenerative mice. PLoS ONE. 2011; 6:e18992. [PubMed: 21559507]
32. Nakano T, et al. Self-Formation of Optic Cups and Storable Stratified Neural Retina from Human ESCs. Cell stem cell. 2012; 10:771–785. [PubMed: 22704518]
33. Evans MJ, Kaufman MH. Establishment in culture of pluripotential cells from mouse embryos. Nature. 1981; 292:154–156. [PubMed: 7242681]
34. Gao G-P, et al. Rep/Cap gene amplification and high-yield production of AAV in an A549 cell line expressing Rep/Cap. Molecular Therapy. 2002; 5:644–649. [PubMed: 11991756]
35. Davidoff AM, et al. Purification of recombinant adeno-associated virus type 8 vectors by ion exchange chromatography generates clinical grade vector stock. J. Virol. Methods. 2004; 121:209–215. [PubMed: 15381358]
36. Luhmann UFO, et al. Differential Modulation of Retinal Degeneration by Ccl2 and Cx3cr1 Chemokine Signalling. PLoS ONE. 2012; 7:e35551. [PubMed: 22545116]
37. Tschernutter M, et al. Long-term preservation of retinal function in the RCS rat model of retinitis pigmentosa following lentivirus-mediated gene therapy. Gene Ther. 2005; 12:694–701. [PubMed: 15660111]

Europe PMC Funders Author Manuscripts

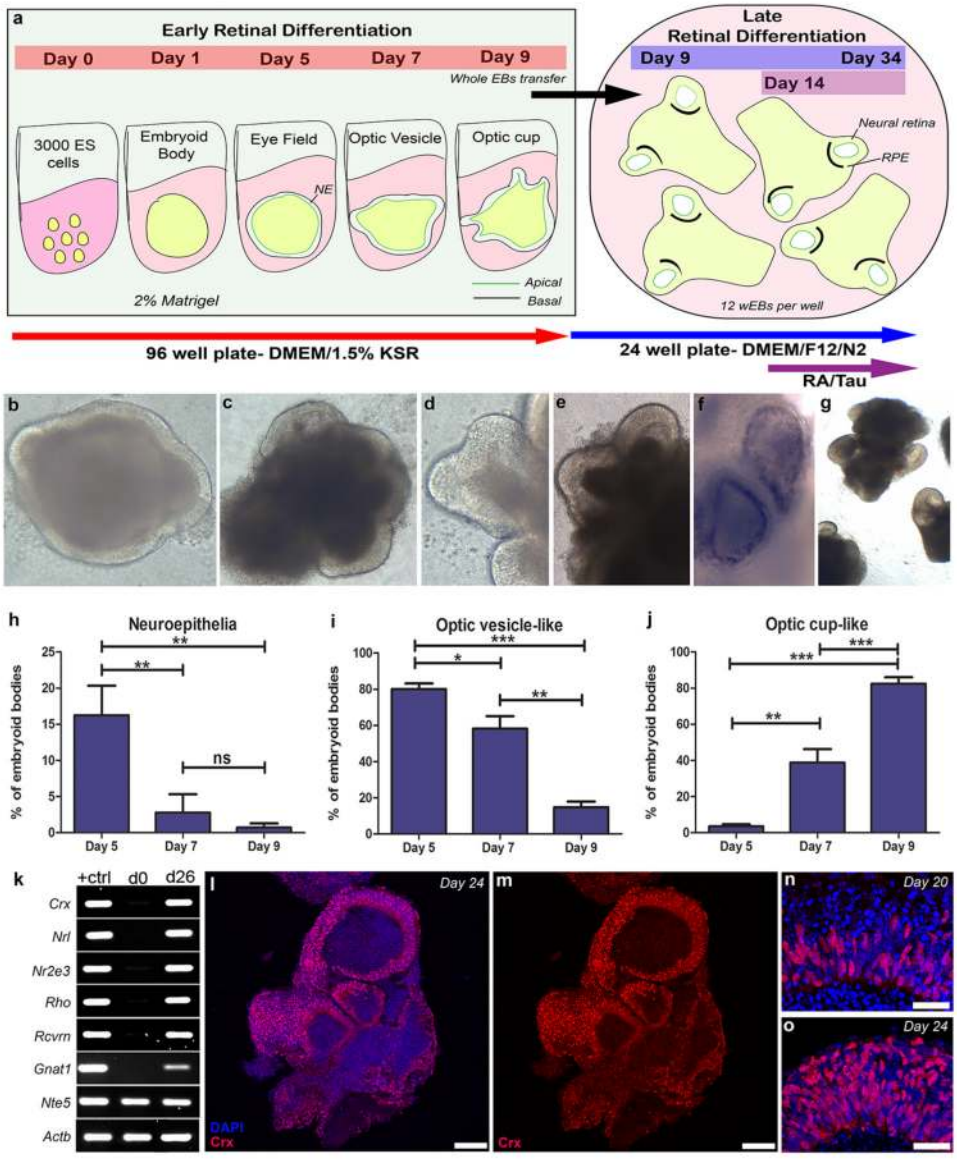

Figure 1. Efficient photoreceptor differentiation in whole EB 3D cultures

a, Schematic of early retinal 3D differentiation showing eye field, optic vesicle and optic cup stages cultured in 96 well plates. Whole EBs (wEB) were transferred from the individual wells at day 9. **b-g,** Representative images of EBs in early stages of retinal differentiation; Neuroepithelium (**b**), optic vesicle (**c**), optic cup–like (**d-e**) stages, wEB showing pigmented RPE at day 12 of differentiation (**f**) and showing transparent optic vesicle in further suspension culture (**g**). **h-j,** Quantification of EBs containing neuroepithelia (**h**), optic vesicle (**i**) and optic cup (**j**) structures. (mean ± SEM, ANOVA, * P<0.05, ** P<0.01, ***P<0.001 N = 4 independent experiments with n = 288 EBs counted per experiment). **k,** RT-PCR analyses showing expression of photoreceptor markers at day 26 of culture. **l,m,** Low magnification image of a wEB showing Crx-positive photoreceptor precursors (red). **n,o,** Neuroepithelium at day 20 and 24 showing increase in Crx positive photoreceptors precursors. Nuclei were stained with DAPI (blue). Scale bars: 25 μm (n,o) and 100 μm (l,m).

Europe PMC Funders Author Manuscripts

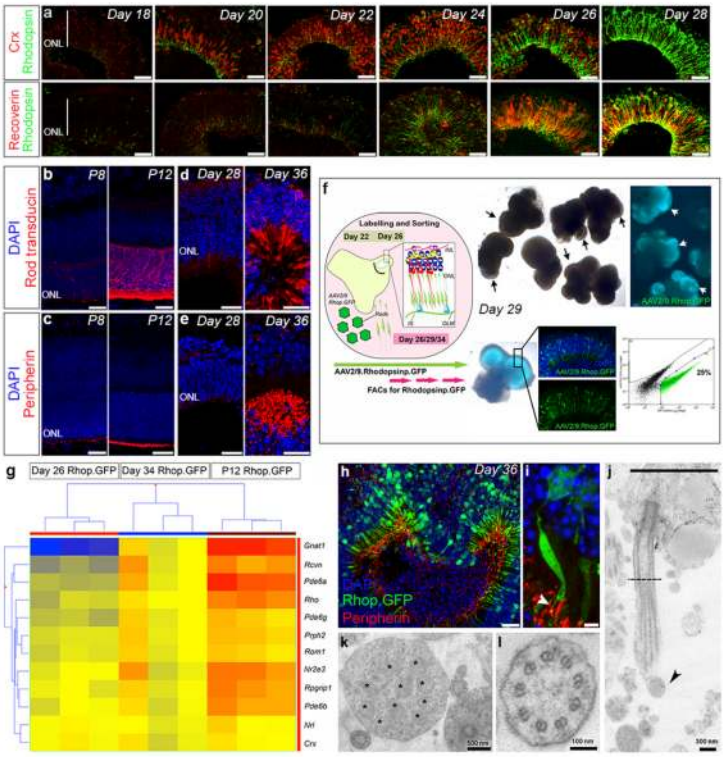

Figure 2. Time course of photoreceptor genesis in whole EB 3D differentiation system

a, Temporal expression of Crx and Rhodopsin (red and green, respectively) and Recoverin and Rhodopsin (red and green, respectively) positive photoreceptors at different time points of culture. **b-e,** Immunohistochemical analysis for Rod -transducin (**b,d,** red) and Peripherin-2 (**c,e,** red) in P8 and P12 retinas and ESC-derived photoreceptors at day 28 and 36 of culture, respectively. **f,** Schematic of viral labelling and FAC-sorting. Light image of day 29 wEBs showing areas of neuroepithelium (black arrows). Fluorescent image of AAV2/9.Rhodopsin.GFP^{+} wEBs (white arrows). Sections confirmed Rhop.GFP^{+} in the neuroepithelium. Representative FACS plot of Rhop.GFP^{+} photoreceptors (green) selected by flow cytometry. **g,** Hierarchical clustering and heat map of 12 photoreceptor associated transcripts at day 26 and 34 ESC-derived and P12 donor-derived Rhop.GFP^{+} cells. **h,i,** Day 36 viral-labeled Rhop.GFP^{+} photoreceptors showing Peripherin-2 (red) at the base of the inner segments. High-magnification of a single Rhop.GFP^{+} photoreceptor stained for Peripherin-2 (**i**, arrow head). **j,** Ultrastructural sagittal section of a day 36 photoreceptor showing inner segment–like (black line), cilium-like (dotted line) structures and the lack of outer segment (black arrow head). **k,l,** Representative images showing transverse sections through an inner segment containing many mitochondria (**k**, asterisks) and a photoreceptor cilium with a 9+0 microtubular organization (**l**). Nuclei were stained with DAPI (blue). Scale bars: 3 m (f), 25 m (a,b,c,e).

Europe PMC Funders Author Manuscripts

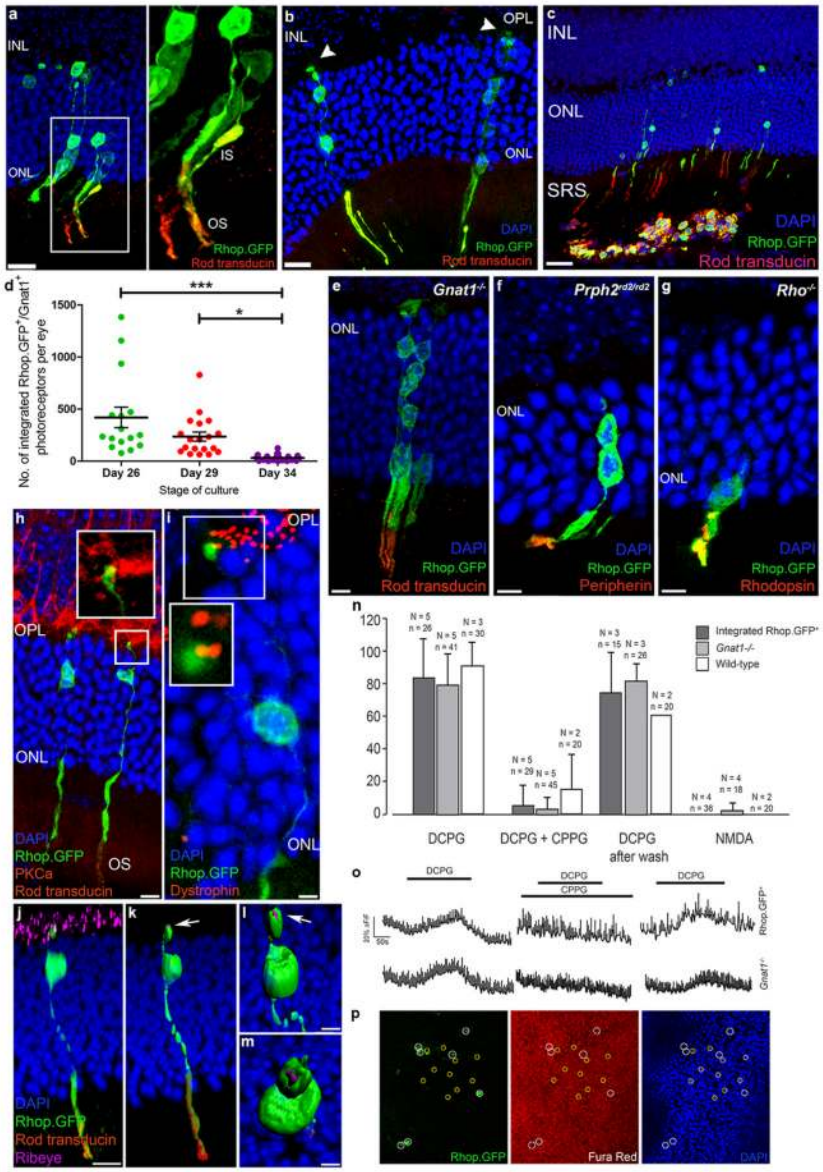

Figure 3. Integration and connectivity of ESC-derived photoreceptor precursors

a,b, Rhop.GFP$^+$ integrated photoreceptors showing mature morphology with outer segments stained for rod α-Transducin (**a,** inset) and spherule formation in the OPL (**b,** arrow head). **c,** Rhop.GFP$^+$/Gnat1$^+$ integrated cells close to the cell mass in the subretinal space (SRS). **d,** Histogram showing the number of Rhop.GFP$^+$/Gnat1$^+$ ESC-derived integrated rods from transplants of days 26, 29 and 34 of culture. **e-g,** Integration of ESC-derived Rhop.GFP$^+$/Gnat1$^+$ photoreceptors into the *Gnat1*$^{-/-}$ (**e**), *Prph2*$^{rd2/rd2}$ (**f**) and *Rho*$^{-/-}$ (**g**) degenerate models as demonstrated by rod α-Transducin, Peripherin-2 and Rhodopsin segment staining, respectively (red). **h,** Rhop.GFP$^+$/Gnat1$^+$ integrated rod spherule in close proximity to bipolar cells (PKC α$^+$, red). **i,** Rhop.GFP$^+$ rod spherule co-localized with ribbon synaptic marker Dystrophin (red). **j,** 3D confocal image of *Gnat1*$^{-/-}$ retinal flatmount showing Rhop.GFP$^+$ integrated rod stained for rod α-Transducin (red) and synaptic marker Ribeye (magenta). **k-m,** 3D reconstruction of the integrated rod highlighting morphology and arrangement of the rod spherule and ribbon synapse. **n,** Intracellular calcium changes in

Europe PMC Funders Author Manuscripts

integrated Rhop.GFP^{+}, *Gnat1*$^{-/-}$ host and WT photoreceptors are similarly evoked by the mGluR8 agonist DCPG and blocked by the specific antagonist CPPG. **o,p,** Mean traces (**o**) of integrated Rhop.GFP^{+} (white circles) and recipient photoreceptors (yellow circles) shown in (**p**). N= number of eyes; n= number of cells imaged. Nuclei were stained with DAPI (blue). Scale bars: 3 μm (i,l,m), 5 μm (e,f,g,j), 10 μm (a,b,h), 25 μm (c).

Europe PMC Funders Author Manuscripts